A high-accuracy wide-angle acoustic system for distance measurements and robot positioning

Ivar Bergkvist

LUND UNIVERSITY

Department of Automatic Control

SONY

Sony Mobile Communications

MSc Thesis
TFRT-6040
ISSN 0280-5316

Department of Automatic Control
Lund University
Box 118
SE-221 00 LUND
Sweden

Printed in Sweden by Tryckeriet i E-huset
Lund 2017

Abstract

Wide-angle distance measurements are needed for positioning with multilateration when there is no information about in which direction objects of interest are located. Several transmitters of varying kinds were evaluated in a data-driven way using a 6 DOF robot actuator. A wide-angle ($\pm$98 degrees) distance measurement system using ultrasound was developed. The resulting solution was integrated in a positioning system showing sub-centimeter accuracy in an industrial environment.

Acknowledgements

Many thanks to my supervisor Peter Isberg for great guidance during the full course of this work. I want to thank Hannes Bergkvist, Mattias Falk and Thomas Fänge for making me a part of the team and for their enthusiastic support. I also want to thank my supervisor Anders Robertsson for providing help and advice.

Contents

1

Introduction

1.1 Background

Accurate positioning pose a challenge for many applications such as robotics, navigation and logistics. One solution is positioning by multilateration, that requires accurate distance measurements. Previous studies have shown high accuracy distance measurements using ultrasound when the transmitters are facing the receiver [Saad et al., 2011]. The use of ultrasound offers the possibility to perform wide-angle distance measurements when there is no information about in what direction an object is located. Systems showing high accuracy at transmission angles up to ± 40 degrees have previously been developed [Medina et al., 2013].

In this work several transmitters have been evaluated at transmission angles up to ± 80 degrees. A final system showing high accuracy positioning at ± 98 degrees is presented accompanied with acoustic theory for better understanding on how accuracy is impacted. The work was conducted at Sony Mobile Communications in Lund, Sweden.

1.2 Objective

The main goal was to develop a robust high-accuracy wide-angle distance measurement system using ultrasound for a commercial positioning system. Based on acoustic features, several distance measuring systems with different transmitters were evaluated in an automated data-driven manner using a robot arm. The evaluation setup is shown in Figure 1.1. The best performing system was integrated in a positioning solution and evaluated in a robot cell in an industrial environment.

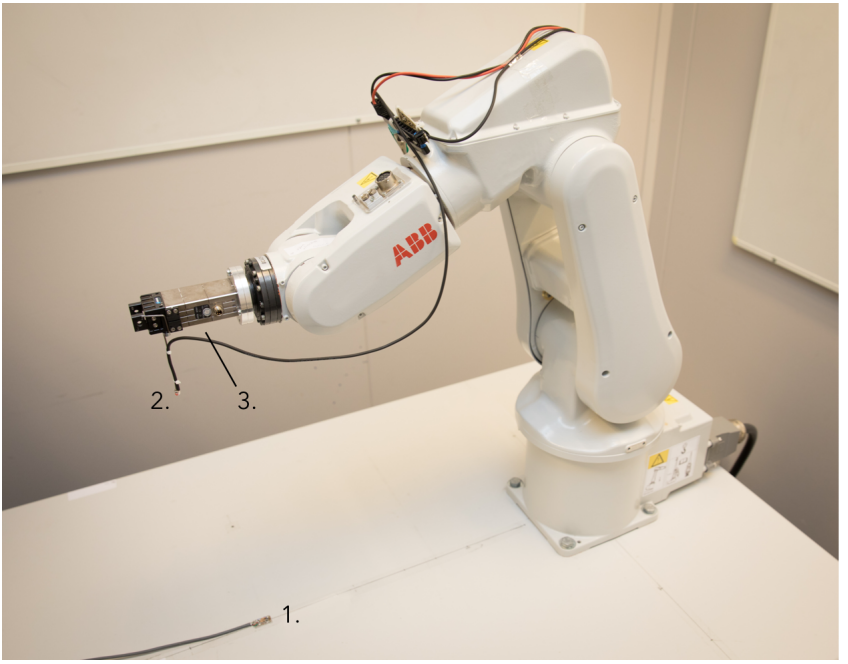

Figure 1.1 Evaluation setup. (1): Microphone. (2): Microphone mounted on the robot. (3): Transmitter mounted on the bottom side of the robot end effector.

2

Theory

2.1 Measurements utilizing the speed of sound

Models

Distance measurements by means of sound are dependent on an accurate value of the speed of sound. The speed of sound in air can be calculated with a simple temperature dependent model shown in Equation 2.1 [Beranek, 1986, p. 10].

$$c = f(T) = 331.4 + 0.6 \cdot T \tag{2.1}$$

where T is the temperature in °C and c is in m/s. To increase accuracy a more advanced model derived from thermo-dynamic relationships can be used, shown in Equation 2.2 [Cramer, 1993].

$$\begin{aligned} c = f(T,p,x_w,x_c) = a_0 + a_1 T + a_2 T^2 + (a_3 + a_4 T + a_5 T^2)x_w \\ +(a_6 + a_7 T + a_8 T^2)p + (a_9 + a_{10} T + a_{11} T^2)x_c \\ +a_{12} x_w^2 + a_{13} p^2 + a_{14} x_c^2 + a_{15} x_w p x_c \end{aligned} \tag{2.2}$$

where T is the temperature in °C, x_w the water vapor mole fraction, x_c the carbon dioxide mole fraction and the constants given in Table 2.1. Equation 2.2 is only valid for temperatures between 0 and 30 °C and pressure range between 60 and 110 kPa. Additional correction may be introduced depending on the frequency of interest.

Table 2.1 Constants for Equation 2.2

a_0	331.5024	a_6	$-1.82 \cdot 10^{-7}$	a_{11}	$5.91 \cdot 10^{-5}$
a_1	0.603055	a_7	$3.73 \cdot 10^{-8}$	a_{12}	-2.835149
a_2	-0.000528	a_8	$-2.93 \cdot 10^{-10}$	a_{13}	$-2.15 \cdot 10^{-13}$
a_3	51.471 935	a_9	-85.20931	a_{14}	29.179762
a_4	0.1495874	a_{10}	-0.228525	a_{15}	0.000486
a_5	-0.000782				

Direct measurement

The speed of sound can be more directly measured if a transmitter and receiver can be moved a known distance relative to each other. By placing a transmitter and receiver facing each other at a 0 degree angle, the time it takes for an acoustic signal to travel between them can be measured. The distance between them can then be calculated using an assumed sound speed. After moving the transmitter a known distance towards the receiver along the 0 degree line to a new position, the new distance can be calculated in the same manner as above. These measurements allow for the speed of sound to be calculated according to Equation 2.3.

$$c = c_a \cdot \frac{\Delta_t}{d_1 - d_2} \tag{2.3}$$

where c_a is the assumed sound speed, Δ_t is the true distance difference, d_1 is the measured distance between transmitter and receiver at the first position, d_2 is the measured distance at the second position.
The method is not dependent on measuring environmental parameters but depends on measuring the time it takes for the sound signal to travel between the transmitter and receiver in an accurate way.

2.2 Sound waves

General

Sound is a pressure disturbance propagating through an elastic material. Considering a gas confined in a container, the pressure on each container surface is dependent on two parameters; the amount of gas particles hitting the surface per unit time and how much momentum each particle transfer to the wall during impact. The amount of particles hitting the surface per unit time can be varied by altering the volume of the container. How the volume is altered impacts how the pressure changes. The temperature, and hence the momentum, of the particles change when the volume is altered. If the volume change occurs slowly, the temperature change has time to dissipate out of the medium and the temperature stays constant. This is called an isothermal process. If the change instead occurs rapidly, an adiabatic process, the temperature change does not have time to dissipate. Since a higher temperature leads to higher pressure, an adiabatic volume change leads to a higher pressure difference than an isothermal volume change. Sound waves are essentially an adiabatic process [Beranek, 1986, p. 5].

Wave equation

The wave equation describing sound pressure waves in three dimensions in a source-free, homogeneous, isotropic, frictionless gas with absorption disregarded is shown

in Equation 2.4 [Beranek, 1986, p. 22].

$$\nabla^2 p = \frac{1}{c^2}\frac{\partial^2 p}{\partial t^2} \tag{2.4}$$

where ∇^2 is the Laplace operator, p is the pressure and c is the speed the wave propagates with.
To further simplify calculations the one-dimensional equation is often considered, as shown in Equation2.5.

$$\frac{\partial^2 p}{\partial x^2} = \frac{1}{c^2}\frac{\partial^2 p}{\partial t^2} \tag{2.5}$$

This is under the assumption that the wave is a plane wave, that is a function dependent on the distance x only. Losses due to dispersion are not taken into account. Considering spherical waves equally radiating in all directions, the equation can be written as Equation 2.6.

$$\frac{\partial^2 p}{\partial r^2} + \frac{2}{r}\frac{\partial p}{\partial r} = \frac{1}{c^2}\frac{\partial^2 p}{\partial t^2} \tag{2.6}$$

where r is the radial distance from the source. The general steady state solution to Equation 2.5 is the real part of Equation 2.7. The solution contains two parts, one describing a wave traveling in the outgoing direction and one traveling in the opposite direction.

$$p(x,t) = \sqrt{2}\,(P_+ e^{ik(ct-x)} + P_- e^{ik(ct+x)}), \qquad k = \frac{2\pi}{\lambda} \tag{2.7}$$

where P_+ and P_- are the RMS (root mean square) sound pressure of the wave traveling in the outgoing and backward direction respectively, c is the speed with which the wave propagates and λ is the wavelength. Considering a freely traveling spherical wave without reflecting surfaces within the medium, the reflected wave traveling in the backward direction can be disregarded and the solution written as Equation 2.8.

$$p(r,t) = \sqrt{2}\,\frac{A_+ e^{-ikr}}{r} e^{-i\omega t} \tag{2.8}$$

where A_+ is the RMS sound pressure magnitude a unit distance from the center and ω is the angular frequency defined as $\omega = 2\pi f$.

Directivity

The size, shape and additional shapes surrounding a sound source determine the directivity of the source. This section considers the far-field behavior, where the distance to the point of measurement is large compared to the size of the source. The energy intensity, I [W/m^2], measured at a distance from the source depends on the directivity of the source. A freely traveling plane wave without dispersion will result in the same energy intensity at any point along the axis of propagation. For

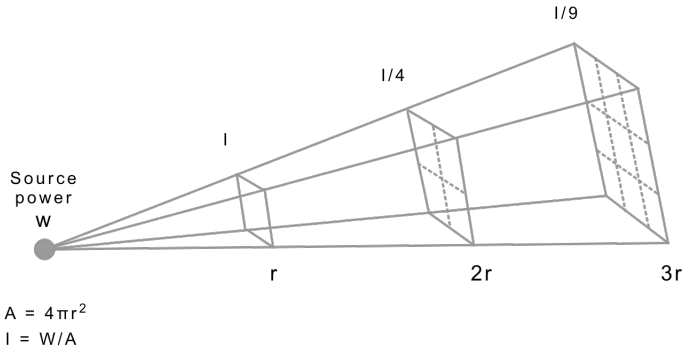

Figure 2.1 Sound energy intensity for a free-progressive spherical wave.

a freely traveling spherical wave the energy intensity at any point is proportional to the inverse square of the radial distance to the center of the source, $I \propto 1/r^2$, as shown in Figure 2.1 where W is the total power emitted from the source and I is the intensity at a distance r from the source. Doubling the distance cuts the energy intensity in four, a 6dB decrease. Since the energy intensity for a free-progressive spherical wave is proportional to the square of the sound pressure, $I \propto p^2$, doubling the distance cuts the sound pressure in half.

A free spherical source with a radius a that is small compared to one-sixth of the wavelength generated ($k \cdot a << 1$), is called a simple source. The simple source is omni-directional, produces spherical waves and can be described with Equation 2.6 and Equation 2.8. The directivity pattern for a simple source is shown in Figure 2.2. The source is located at the center of the figure and the black line is the measured sound pressure at different angles compared to the sound pressure at the zero degree angle [Beranek, 1986, p. 92]. Though sending a signal uniformly throughout a volume might be convenient if the location of the receiver is not known, it demands higher output to reach the same energy intensity compared to a directed signal. For a frequency of 20 kHz the wavelength is 17 mm and the source has to have a radius small compared to 2.8 mm to be a simple source. The need for high output combined with a small physical size pose a practical problem that increases in difficulty with decreasing wavelength.

Other shapes can be described by dividing the shape into small elements, each of which is a simple source in phase with the others. The sound pressure for the shape is the combined sound pressure for all the elements of the source. Using this method it can be shown that a freely suspended thin rigid piston can be approximated as two simple sources with opposing phase located close to each other, known as a doublet sound source. The directivity is identical for the forward and backward traveling sound waves generated. The directivity in both directions nar-

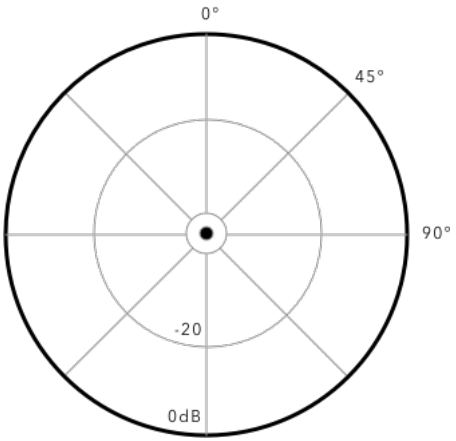

Figure 2.2 Directivity pattern for a simple source. The sound pressure is equal at all angles.

row as the product of $k \cdot a$ increases.

By placing a rigid piston at the end of a long tube, the rear side of the piston can be isolated from the front side. By dividing into simple sources and summing the contribution as described above, the directivity pattern for the construction can be determined. It is however more complex as the effects of diffraction around the tube corners have to be considered. It can be shown that for $k \cdot a < 0.5$ the construction is very much omni-directional and as the product of $k \cdot a$ increases the sound wave is focused in the forward direction.
If instead a piston placed in an infinite baffle is considered, the diffraction around the edges can be omitted while the rear side of the piston still is isolated from the front side. Just as for the piston in a tube, the construct acts like an omni-directional source when the product of $k \cdot a < 0.5$. The difference being that it can only be omni-directional in a hemispherical way as the baffle hinders any wave from passing in a backwards direction. As the product of $k \cdot a$ increases so does the directivity of the wave as shown in Figure 2.3.

Acoustic center

The acoustic center is the point from which spherical sound waves from an acoustic transducer seems to be diverging. It determines the point of origin and point of reception for acoustic transducers. This point can appear to be outside the physical borders of the transducer. How well it is defined impacts the accuracy of measurements. When it is not possible to measure the acoustic center, decreasing the size of the transmitter and receiver should decrease the unambiguity of where the acoustic center is located.

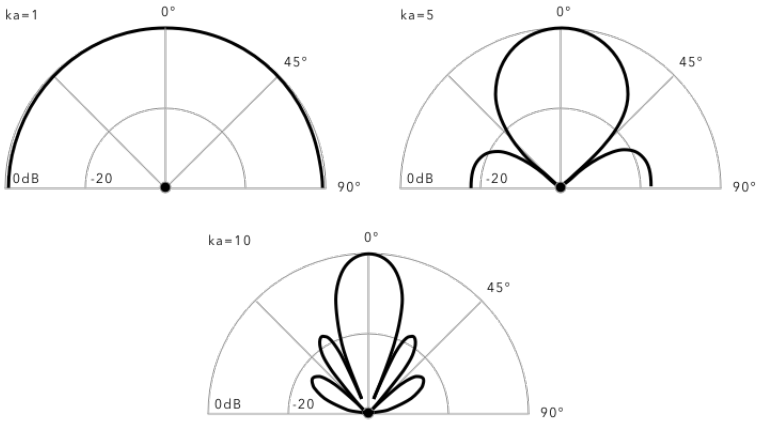

Figure 2.3 Directivity pattern for a rigid piston in an infinite baffle with different values on $k \cdot a$.

Acoustic impedance

Acoustic impedance is a complex-valued quantity that expresses how difficult a medium is to move at a certain frequency. *Specific* acoustic impedance, Z_s, is defined as shown in Equation 2.9

$$Z_s(f) = \frac{p(f)}{u(f)} \tag{2.9}$$

where f is the frequency, p is the effective sound pressure at a point of an acoustic medium, u is the effective particle velocity at that point and the unit is Ns/m^3. By taking the average effective sound pressure over a surface and the average effective volume velocity through it, acoustic impedance can be defined as shown in Equation 2.10

$$Z(f) = \frac{P(f)}{U(f)} \tag{2.10}$$

The unit for acoustic impedance is acoustic ohms [Ns/m^5]. A low acoustic impedance means the medium moves easily when a pressure is applied. The real part of the acoustic impedance accounts for the power radiated from the medium when vibrating. The imaginary part is related to the power stored within the near field of the source of vibration [Kleiner, 2013, p. 166].

Reflection

When a sound wave encounters a shift in acoustic impedance, a part of the wave will be reflected and the rest will continue onwards. The cause of the impedance shift can be due to physical phenomena such as temperature or pressure shifts within

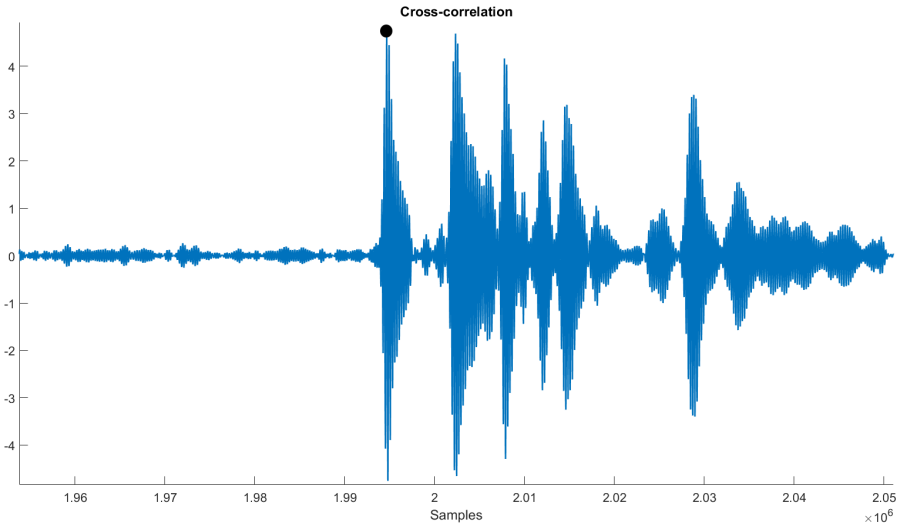

Figure 2.4 Plot of cross-correlation between sent and received signal. After the cluster of peaks for the direct wave marked with a black dot, additional clusters for reflecting waves appear.

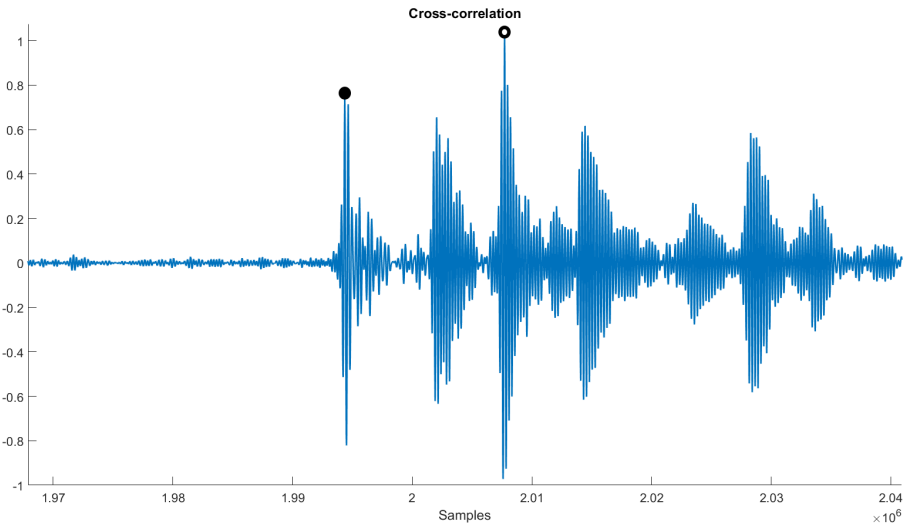

Figure 2.5 Plot of cross-correlation between sent and received signal. The cluster of peaks for the direct wave marked with a black dot, has lower amplitude than one of the clusters of peaks due to reflections marked with a hollow dot.

the medium, or it can be caused by the encounter of a different medium all together. How much of the wave that is reflected is determined by the angle the wave encounters the impedance shift with and how the impedances of the mediums differ [Kleiner, 2013, p. 25]. When using acoustic signals for distance measurements, reflections can cause some issues. A reflected wave will show up as distorted repetitions on the receiving side as shown in Figure 2.4. With one or more reflective surfaces the reflected signals can by constructive interference add up to become stronger than the direct wave causing false a maximum in signal processing methods such as cross-correlation or similar as shown in Figure 2.5. An obstructed path for the direct wave can lead to similar issues. Depending on the type of microphone used, care must be taken so the mounting structure or surface do not cause interference due to reflections.

Absorption

Spherical waves drop in intensity as described in Section 2.2. When sound waves travel through a medium some energy will be absorbed as well. For air, this is dependent on both frequency and relative humidity as shown in Figure 2.6. For a 20 kHz plane wave at 20 degrees Celsius in dry air, the sound pressure will be attenuated ~0.7 dB at a distance of 10 m. For a 20 kHz plane wave at 20 degrees Celsius and 40 % relative humidity, the sound pressure will be attenuated ~6 dB at a distance of 10 m [*Engineering Acoustics/Outdoor Sound Propagation - Wikibooks, open books for an open world*].

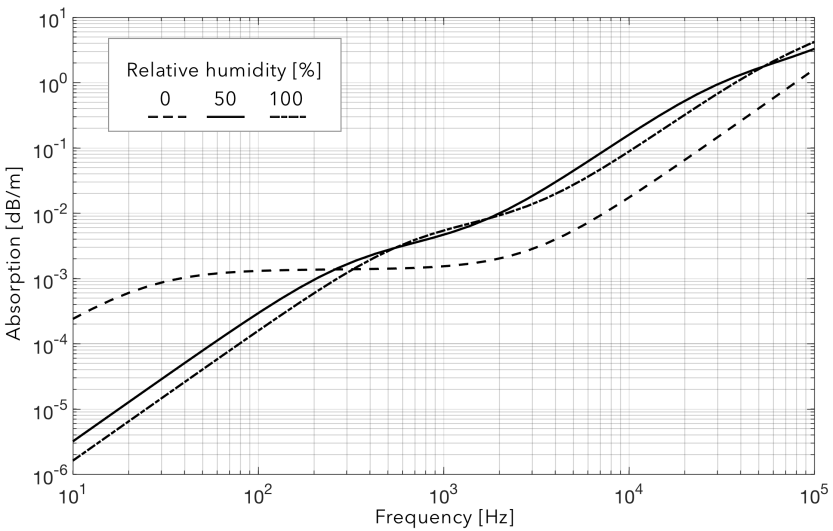

Figure 2.6 Sound attenuation for air at 20 degrees Celsius. Drawn for different frequencies and varied relative humidity.

2.3 Transmitters

Electrodynamic speaker

An electrodynamic speaker usually consists of a permanent magnet and a coil where the magnetic forces between them drive a diaphragm. A charged particle traveling through a magnetic field will experience the Lorentz force according to Equation 2.11. Considering a current flowing through a wire in a magnetic field, the force on the wire can be calculated according to Equation 2.12 By varying the magnitude and direction of the current, the force acting on the wire can be modulated. Electrodynamic speakers exploits this phenomenon by attaching a diaphragm to a coil suspended in the magnetic field from a permanent magnet. As the current through the coil is changed the coil and diaphragm move accordingly, compressing and decompressing the adjacent medium, causing sound.

$$F_p = q(v \times B) \tag{2.11}$$

where F_p is the force acting on the charged particle in Newton, q is the charge of the particle in Coulomb, v is the velocity of the particle in m/s and B is the magnetic field in Tesla.

$$F_w = l(I \times B) \tag{2.12}$$

where F_w is the force in Newton acting on the wire, B is the magnetic field in Tesla, I is the current in Ampere and l is the length of the wire carrying the current in meters.

The material suspending the coil and diaphragm introduces a restoring force proportional to the displacement caused by the Lorentz force. The constant describing the proportionality is called stiffness. With the addition of the mechanical dampening such as friction in the suspension and the electrical dampening due to electromagnetic braking, the system acts as a damped spring-mass system described with Equation 2.13.

$$F(t) - k \cdot x - c \cdot \frac{dx}{dt} = m \cdot \frac{d^2x}{dt^2} \tag{2.13}$$

where F is the driving force, k is a constant depending on the suspension of the membrane, c is the vicious damping constant and m is the mass of the oscillating parts. The Q-value of the speaker is defined as the mechanical and electrical dampening combined.

The system acts differently depending on the frequency of the driving signal as shown in Figure 2.7. For frequencies below the resonance frequency, the acceleration of the coil and diaphragm is small. The system is mainly controlled by the stiffness, and the inertial mass of the moving system does not play a major factor. At frequencies higher than the resonance frequency, the acceleration of the coil and diaphragm is large. The force needed to achieve high enough acceleration to accurately reproduce the signal is dependent on the inertial mass of the accelerating

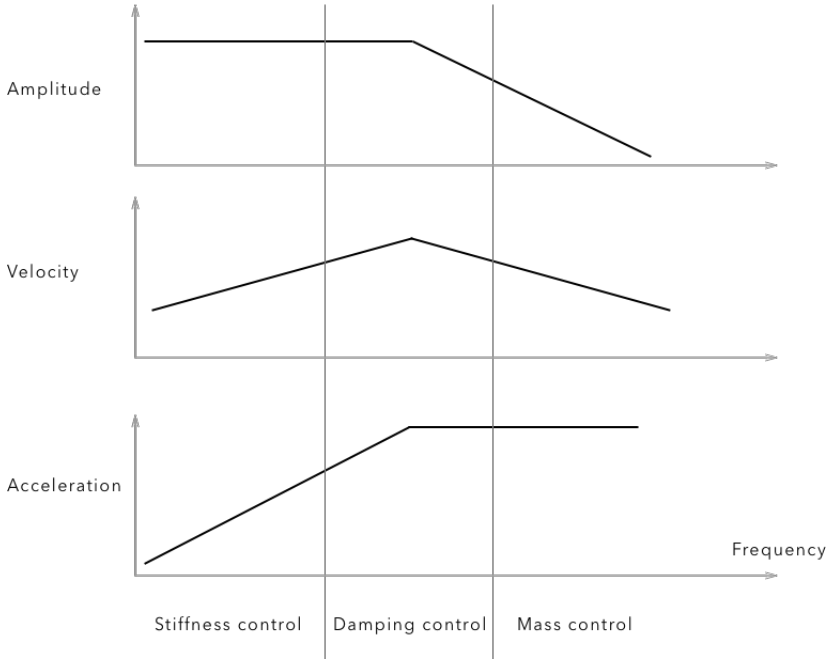

Figure 2.7 Displacement, velocity and acceleration for a simple mass-spring system, e.g., an electro-dynamic speaker element. When mounted in a closed box, the sound pressure at a distance is proportional to the acceleration of the membrane, (approximation for wavelengths small compared to the size of the speaker box).

system as described in the Newton second law. The force needed to overcome the stiffness of the system becomes a less prominent factor and the system is said to be mass-controlled. If the speaker is mounted to the side of a closed box the air trapped inside the box will act as a spring introducing an additional restoring force. When the diaphragm of the speaker moves inwards the air within the box is compressed. The pressure difference between the inside and the outside of the box creates a force directed to restore the diaphragm to the initial position. When the diaphragm moves outwards it will experience a restoring force due to the same phenomenon but with a pressure decrease inside the box. The additional restoring force due to the box increases the stiffness of the speaker.

Piezoelectric transmitter

A piezoelectric material is characterized by the property that if exerted to a suitable force, an electrical charge is distributed on the surface. The piezoelectric effect is reciprocal, so by applying an electric charge on the surface, the material is deformed [Kleiner, 2013, p. 153]. Piezoelectric transmitters leverage the piezoelectric effect

to turn electrical signals into movement used to produce sound waves. Since the deformation is small and the acoustic impedance of piezoelectric materials is much higher than the impedance of air, a mechanical impedance matching is often used.

The electrical energy is directly transformed into physical movement enabling transmitters with high efficiency. The piezoelectric transmitter can be described with Equation 2.13 but with the constant k decided by the crystal properties. Since the whole material is deformed when producing sound, the moving mass is large. With low damping this can lead to ringing phenomenas measured as high Q-values. Each piezoelectric transmitter has a resonance frequency often defined by the mechanical amplification. For wide-band applications such as speakers for music, transmitters with resonance frequency above the frequencies of interest are often used to provide a flat frequency response. For other applications such as beepers and alarms, the transmitter resonance frequency can be tuned to a desired frequency as a way to improve efficiency. Piezoelectric transmitters come with the advantage that they can be produced in a variety of shapes such as spheres, hemispheres, cylinders and similar.

Corona transmitter

A Corona discharge is formed in air when an electric field is strong enough to ionize the air molecules around an electrode but not strong enough to cause electrical breakdown and form an arc. The produced positive ions and negative electrons will drift in opposite directions creating a current, hence the discharge. By modulating the electric field, the ion cloud around the electrode can be made to oscillate in a way as to create sound [Chizhov et al., 2013]. The electrical signal is directly transfered to the air and the transmitter is a so called "membrane-free" acoustic system and is not mass- and stiffness-controlled in the same way as electrodynamic and piezo transmitters but can be described by a hydrodynamic model of a weakly ionized gas [Chizhov et al., 2013]. By varying the shape of the electric field, the ion cloud could be formed as a sphere making the produced sound waves look like they origin from a single point from afar.

2.4 Receivers

Dynamic microphones

A dynamic microphone works like an electrodynamic speaker in reverse. When sound waves hit the diaphragm it sets the coil in motion. Moving the coil in the static magnetic field changes the magnetic flux within the coil and induces an electromotive force according to Faraday's law shown in Equation 2.14

$$F_{emf} = -N\frac{d\Phi}{dt} \tag{2.14}$$

where N is the number of loops of the coil and ϕ is the magnetic flux within the loops of the coil.

Electrostatic microphones

Electrostatic microphones are based on measuring the capacitance difference between a charged membrane and a backplate. When sound waves hit the membrane it moves, causing a change in capacitance that can be measured. MEMS (microelectro-mechanical systems) are usually miniature electrostatic microphones produced by etching a pressure sensitive diaphragm directly to a silicon wafer. Since the membrane has a very small mass, a small force is enough to accelerate the membrane. Hence it stays in the stiffness-controlled region for high frequencies making it a good fit for ultrasonic applications.

Piezoelectric microphones

In the same way as applying a voltage over a piezoelectric material causes the material to deform, physical pressure deforming a piezoelectric material causes a voltage. A piezoelectric microphone measures the voltage caused when acoustic waves deform a piezoelectric material. Just as for piezoelectric transmitters the whole piezoelectric material is oscillating which can lead to ringing phenomenas due to the large mass.

2.5 Porting

Impedance matching

In the case of a rigid piston and air the impedance is poorly matched. Maximum power is radiated when the impedance of the source is the conjugate of the impedance of air [Kleiner, 2013, p. 168]. To achieve higher acoustic energy throughput a structure in front of the membrane can be introduced. A common solution is the horn shown in Figure 2.8. Close to the speaker the air movement is limited to the forward direction by the horn. This makes the air harder to move as it can not disperse to the side as is possible when a flat baffle is used. The confined air has a higher impedance which is closer to the impedance of the speaker. As the horn widens the air is less constrained and the impedance drops gradually until it reaches the same value as free air at the end.
It is also possible to add a physical layer that has a more similar impedance to the air directly to the transmitter. This is more common with piezoelectric transmitters where the matching layer also can be used to tune the resonance frequency.

With better impedance matching more energy will be radiated. The mass of the immediate adjacent medium that oscillates in phase with the transmitter adds to the effective mass of the transmitter. This lowers the frequency where the system becomes mass-controlled.

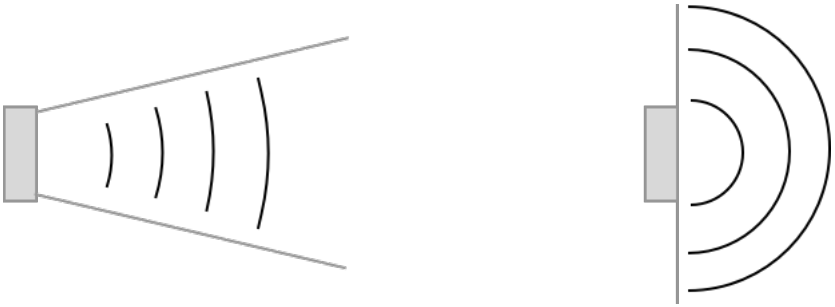

Figure 2.8 Speaker mounted with conical horn (left) and flat baffle (right).

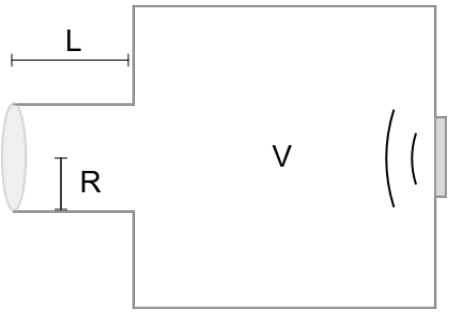

Figure 2.9 Speaker mounted with a Helmholtz resonator with neck length L, neck radius R and chamber volume V.

Resonator

A front cavity can be used to achieve resonance for a desired frequency as a way to amplify it. The Helmholtz resonator, shown in Figure 2.9, is a well known construct to amplify a single frequency. It acts as a second-order low-pass filter. Equation 2.15 can be used to calculate the resonance frequency for the Helmholtz resonator

$$f = \frac{C}{2\pi}\sqrt{\frac{A}{VL}} \tag{2.15}$$

where C is the speed of sound, V is the volume of the chamber, L is the length of the neck and $A = \pi \cdot R^2$ is the cross-sectional area of the neck as depicted in Figure 2.9.

2.6 Signal processing

Sampling

To fully represent a signal in PCM (pulse-code modulation) format, care must be taken to sample it sufficiently often. To avoid aliasing the Nyquist sample rate criterion should be fulfilled [A. Olshausen, 2000]. The time between samples should be accurately identical to assure each sample is correctly timed meaning a high-accuracy clock with low jitter is needed. At least one period of the lowest frequency must be fully sampled to accurately capture the signal. Hence, longer sampling times are needed for lower frequencies.
The bit depth controls the accuracy of the sound pressure recorded at each sample. Noise will be introduced due to the quantization of the signal into bits. The SNR (signal-to-noise ratio) is a measure of the ratio between the signal strength and the noise, in this case the noise introduced due to the bit rate quantization error from the sampling process. Considering a full scale sinusoid, the SNR can be approximated with Equation 2.16 [Kester, 2004].

$$SNR = 6.02Q + 1.76dB \tag{2.16}$$

where Q is the number of bits used for the quantization and SNR is in dB. Common bit depth values are 16 and 24 bits leading to 98 and 146 dB SNR.
When a signal is sufficiently sampled all information needed for it to be reconstructed is known. To increase the sample rate, and hence the number of samples that can be investigated, the signal can be up-sampled. The process can be summarized in two steps. First a constant set of zeros is introduced in between each sample. Thereafter the new signal is passed through a low-pass filter that smooths out the discontinuities [Oppenheim et al., 1999, p. 172].

Time estimate

The distance between an acoustic transmitter and receiver can be determined if the time it takes for the signal to travel between them is known. By letting the receiver start recording at the same time as the transmitter starts transmitting, the time difference between the signals can be determined by cross-correlating the signals. A visual description of cross-correlation is shown in Figure 2.10 The received signal R (red) is offset and multiplied with the transmitted signal T (blue) producing a resulting signal (green). The area under the green signal is recorded as the correlation value for that offset. The offset is changed and the area under the new resulting signal is calculated. The offset producing the largest cross-correlation value corresponds to the time it takes for the signal to travel between the transmitter and receiver. Cross-correlation can also be described as in Equation 2.17

$$(T \cdot R)[n] = \sum_{n=-\infty}^{\infty} T^*[m]R[m+n] \tag{2.17}$$

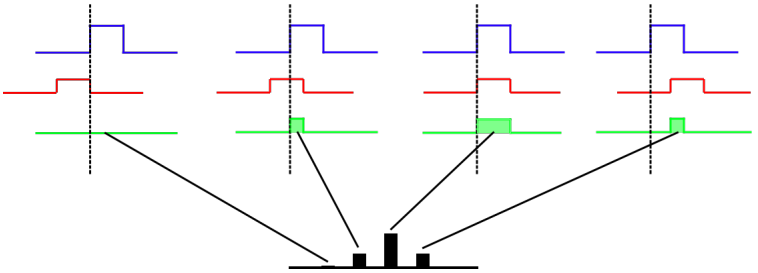

Figure 2.10 Cross-correlation to determine the time offset between transmitted and recorded signal

where T^* is the complex conjugate of T and m is the sample offset.
The Hilbert transform can be used to create an analytic signal [“Technical Review To Advance Techniques in Acoustical, Electrical and Mechanical Measurement - The Hilbert Transform”, p. 10]. By using the Hilbert transformation the propagation time can be estimated even if it does not correspond to the maximum peak of the cross-correlation [“Practical use of the "Hilbert transform"”].

2.7 Positioning

If the transmitter can be moved to three or more known positions, the position of the receiver can be calculated. In two dimensions, each distance measurement from a known position constrains the possible positions of the receiver to a circle centered around the known position. After multiple measurements the position of the receiver can be determined as shown in Figure 2.11. Care must be taken to not use known positions on a straight line as this leads to ambiguous results as shown in Figure 2.12. In two dimensions three correctly configured known points and their individual distance to the point of interest is enough to determine the position unambiguously. In three dimensions at least four known positions are needed. With perfectly known positions and distances the position of the receiver can be analytically solved. With the addition of measurement errors numerical methods are better suited. There are several numerical methods such as the iterative least squares method [Ali-Löytty et al., 2010] and particle filters [Thrun et al., 2005] which are out of the scope for this paper.

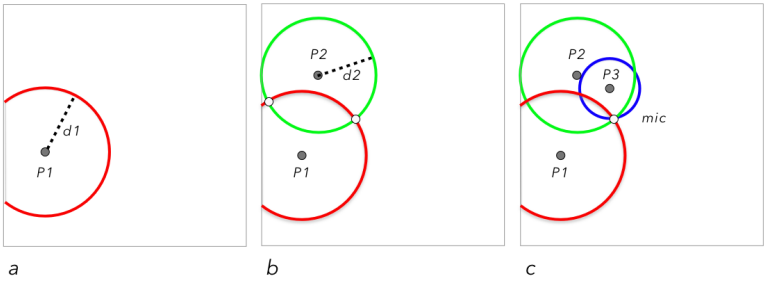

Figure 2.11 Trilateration in 2D. (a): After a first distance measurement, $d1$, the position of the receiver is constrained to the red circle with the distance as radius. (b): After a second measurement, $d2$, the position of the receiver is further constrained to the intersection of the red and green circle. (c): A third measurement completely determines the position of the receiver.

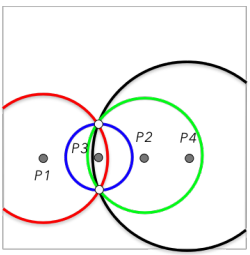

Figure 2.12 Trilateration in 2D with known points on a straight line.

3

Acoustic components

3.1 Transmitters

Nine different transmitters were used. This section gives a brief summary of their specifications.

Piezo 1

Piezo 1 is a dedicated ultrasound piezo-transmitter with resonance frequency at 25 kHz. It has a specified SPL of 112 dB at 30 cm, 10 Vrms, 25 kHz and a transmission angle of ± 42.5 degrees. It has a membrane diameter of 13 mm.

Piezo 2

Piezo 2 is a dedicated ultrasound piezo-transmitter with resonance frequency at 40 kHz. It has a specified SPL of 100 dB at 30 cm, 10 Vrms, 40 kHz and a transmission angle of ± 62.5 degrees. It has a transmitting surface with a diameter of 8 mm.

Piezo 3

Piezo 3 is a dedicated ultrasound piezo-transmitter with resonance frequency at 40 kHz. It has a specified SPL of 106 dB at 30 cm, 10 Vrms, 40 kHz and a transmission angle of ± 60 degrees. The transmitter is enclosed in a plastic cap with a diameter of 18 mm.

Piezo 4

Piezo 4 is a dedicated ultrasound piezo-transmitter with resonance frequency at 40 kHz. It has a specified SPL of 120 dB at 30 cm, 10 Vrms, 40 kHz and a transmission angle of ± 40 degrees. It has a membrane diameter of 7 mm.

Piezo sphere

The piezo sphere was not obtained as an off-the-shelf transmitter, but rather as a component to be used in sonar equipment or medical devices. Hence the acoustic properties in air were not disclosed.

Speaker 1

Speaker 1 is an electrodynamic speaker with resonance frequency at 850 Hz and has a specified SPL of 87 dB at 10 cm, 0.3 W, 2 kHz. The speaker is constructed for the audible area and specifications for ultrasound frequencies are not disclosed. It has a membrane 13 mm in diameter. The transmission angle is not disclosed (depends on the enclosure).

Speaker 2

Speaker 2 is an electrodynamic speaker with resonance frequency at 1050 Hz and has a specified SPL of 86 dB at 10 cm, 0.2 W, 3 kHz. It has a membrane 13 mm in diameter. The transmission angle is not disclosed (depends on the enclosure).

Speaker 3

Speaker 3 is an electrodynamic speaker with resonance frequency at 1300 Hz and a specified SPL of 86 dB at 10 cm, 0.1 W, 2 kHz. It has a membrane 10 mm in diameter. The transmission angle is not disclosed (depends on the enclosure).

Corona discharge

A slayer-exciter electronic circuit was used to produce a modulated corona discharge around the tip of a 0.13 mm copper wire. The corona discharge is further discussed in Appendix A.1

3.2 Receivers

MEMS microphones were used as they provide a small point of reception allowing for high accuracy. The microphones used are specified for usage in the ultrasound frequency band and are omni-directional as well as cheap and easily obtained. One digital and one analog type were used.

Microphone 1

Microphone 1 is an omni-directional analog MEMS microphone with a sensitivity of -38 dB. It is designed for ultrasound frequencies. The entry port diameter is 0.25 mm. The frequency response for Microphone 1 is shown in Figure 3.1. Within 20-45 kHz, it has an estimated noise level equivalent of 34 dBSPL, with the assumption that the noise is white.

Microphone 2

Microphone 2 is an omni-directional digital MEMS microphone with a sensitivity of -26 dB and is designed for ultrasound frequencies. The entry port diameter is 0.25 mm. The frequency response for Microphone 2 is shown in Figure 3.2

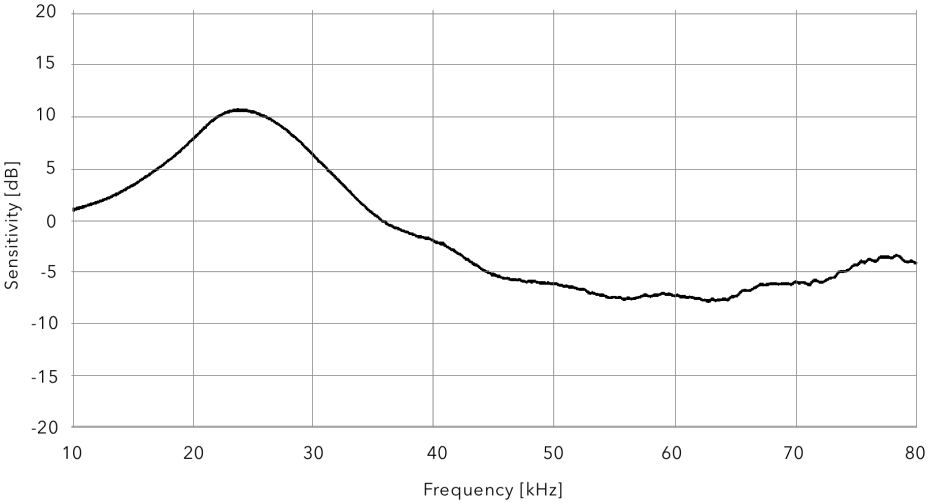

Figure 3.1 Frequency response for Microphone 1.

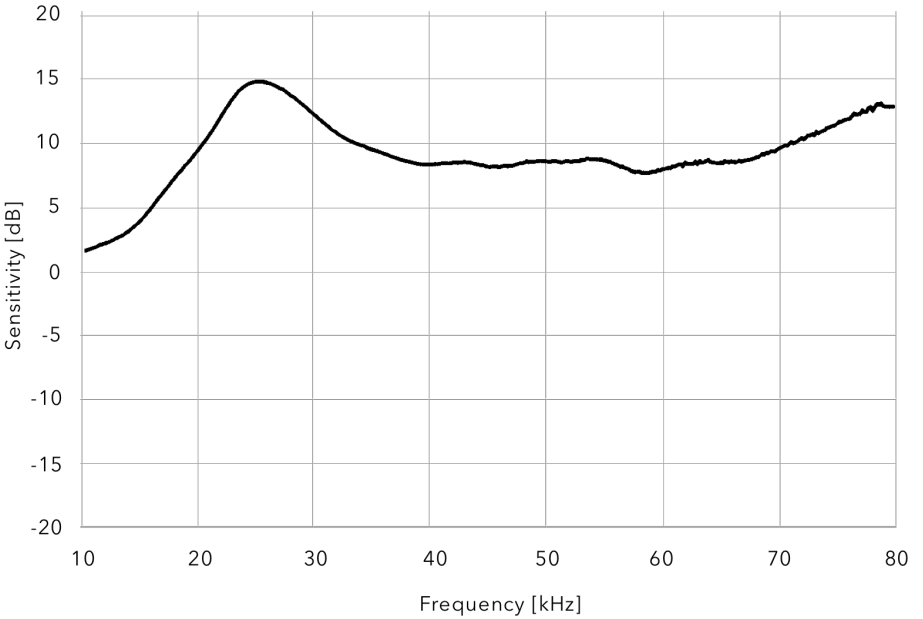

Figure 3.2 Frequency response for Microphone 2.

4

Evaluation process

4.1 Transmitter comparison

Objective

The objective of the transmitter comparison procedure was to evaluate how each transmitter performed as a part of the distance measurement system and compare the results in a data-driven way. The main performance features were repeatability, standard deviation and absolute error of the measurements performed with the transmitter on- and off-axis at varying distances relative to the receiver.

Process

The process took place in a small office room, $3.5 \times 2.2 \times 2.7$ m^3, with a thin carpet, acoustic ceiling absorbers, furniture and one robot arm with controller as shown in Figure 4.1. The process used for evaluating a transmitter for the distance measurement solution is described below. All positions refer to positions defined in the robot coordinate system. The transmitter was mounted at the end effector of a 6 DOF (degrees of freedom) robot arm with as few obstructing parts as possible. An analog MEMS microphone was mounted at the end effector in close proximity to the transmitter. Two additional analog MEMS microphones were fixed at two different positions with known coordinates in the room. The microphones were connected to a professional sound card [*RME: Fireface UFX*] interfaced with Matlab [*MATLAB R2016b*]. The transmitter was connected to the sound card through a variable amplifier. Each transmitter was tested at the specified max continuous VRMS.
A weather station recorded the temperature, humidity and pressure, and the speed of sound was calculated according to Equation 2.2 [*BME280*]. The robot positions were calculated with a Python script that controlled the robot through a Python-Rapid API [*open_abb* 2017]. The robot was moved to place the transmitter at a known position and orientation. A distance measurement was performed as follows.
The transmitter sent a pseudo-random noise signal. The electrical signal to the

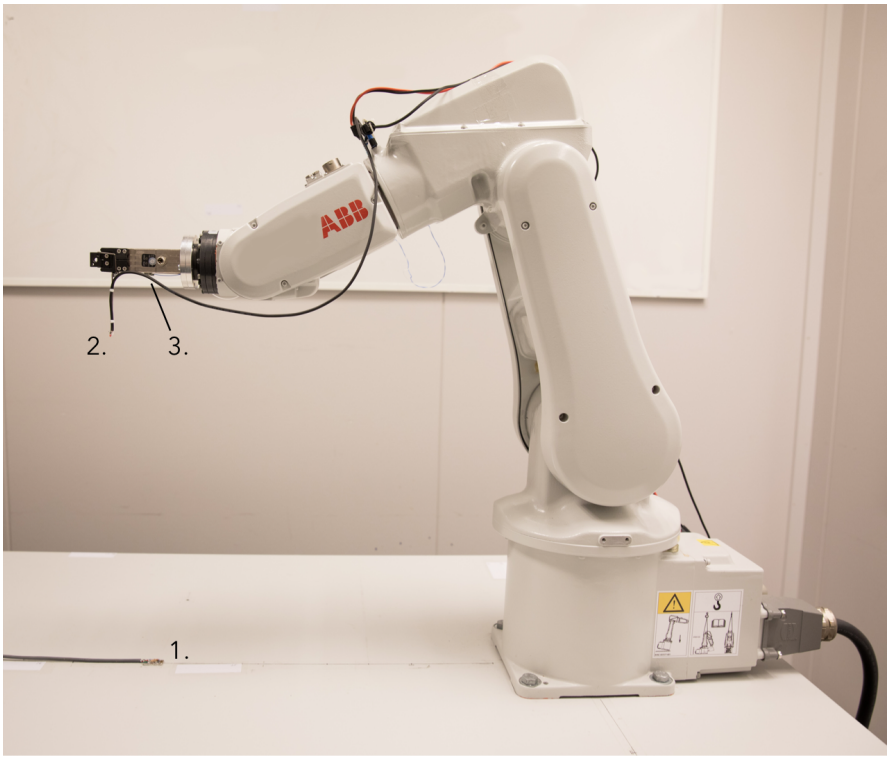

Figure 4.1 Evaluation setup. (1): Microphone. (2): Microphone mounted on the robot. (3): Transmitter mounted on the bottom side of the robot end effector.

transmitter, the recorded signal from the microphone mounted on the robot and the signal recorded at one of the microphones in the room were simultaneously recorded for 200 ms. Which microphone in the room that was used depended on the test case. A sampling rate of 96000 samples per second was used.
The captured signals were put through the signal processing algorithm described in the next section and the distance between the transmitter and microphone was determined. Values outside $1.5 \cdot \text{IQR}$ (interquartile range) were considered outliers and were removed. The true distance between the transmitter and microphone was known from their positions. The calculated distance was compared to the true distance. Repeatability, standard deviation and absolute error were calculated.
The procedure was repeated for 31 unique positions with 100 measurements at each position. The positions are shown in Figure 4.2.

Further description of Figure 4.2.
1: Fixed angle with varying height, h, between 400 mm and 100 mm at 50 mm

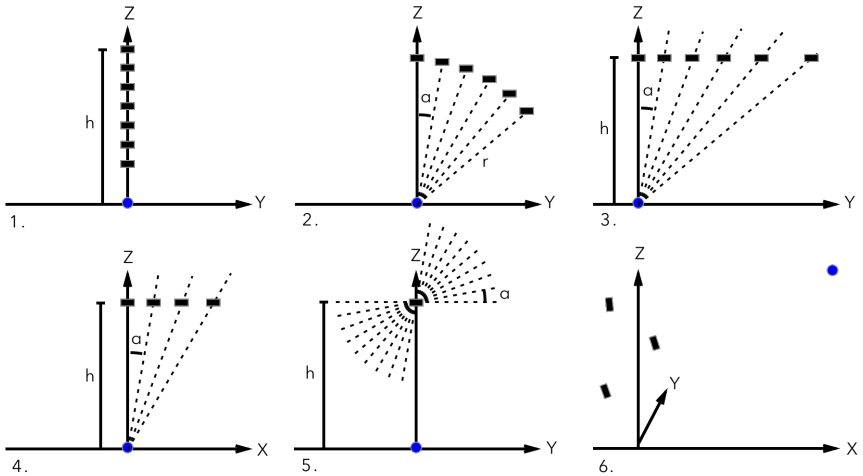

Figure 4.2 Evaluation positions. Transmitter positions depicted as a black rectangle and microphone position depicted as a blue circle.

steps.
2: Fixed radius, r, at 300 mm with angle α between 0 and 50 degrees with 10 degree steps.
3: Fixed height, h, at 300 mm with angle α between 0 and 50 degrees with 10 degree steps moving along the y-axis.
4: Fixed height, h, at 300 mm with angle α between 0 and 30 degrees with 10 degree steps moving along the x-axis.
5: Fixed height, h, at 300 mm. Varying orientation angle α of the transmitter between 0 and 80 degrees with 10 degree steps.
6: Range test. Transmitter at three different positions, directed at the second microphone mounted further away.

Each transmitter went through the same evaluation process. After a transmitter had been fitted to the robot arm and the robot tool had been adjusted to account for the physical dimensions of the transmitter, the evaluation process was fully automated.

Distance estimation

The recorded signal was cross-correlated with the reference signal. Two cases were evaluated. Using the electrical signal to the transmitter as reference signal and using the signal recorded with the microphone close to the transmitter as reference signal. The correlation signal was up-sampled ten times to increase the granularity of the sample delay and the absolute value was calculated. The maximum correlation peak was identified. An early peak search was performed where the earliest peak reaching

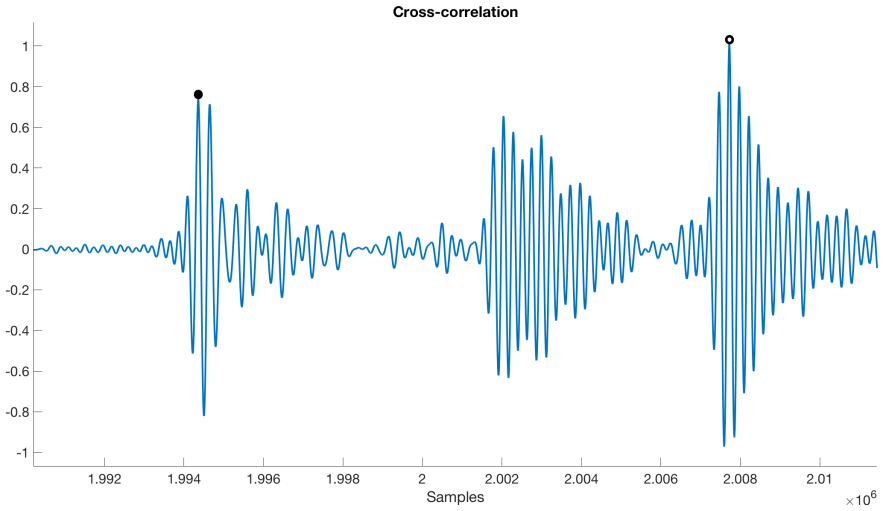

Figure 4.3 Cross correlation. Max value marked with a hollow black dot and earliest peak marked with a solid black dot.

70 % of the max peak value was chosen to avoid strong peaks due to reflections. The sample delay of the identified earliest peak was converted to a distance with use of the previously recorded sound speed and known sample rate. Figure 4.3 shows the cross-correlation plot for a transmitter with the correlation max value marked with a hollow black dot and the earliest peak marked with a solid black dot.

4.2 Industrial environment evaluation

Objective

For the industrial environment evaluation Piezo 2 was used. The objective was to measure how the distance measuring system preform as a part of a positioning system in an industrial environment.

Process

The evaluation took place at a robot research facility in a noisy environment containing several robot controllers and other mechanical tools [*Robotdalen*]. The microphones and transmitter were mounted on separate PCBs, (Printed circuit boards) equipped with radio transceivers and the capability of time synchronization between the transmitted and recorded signal. The PCBs were mounted in plastic casings with a microphone port as shown in Figure 4.4. Communication was wireless and cables were used for power supply only. Six microphones were placed within a volume

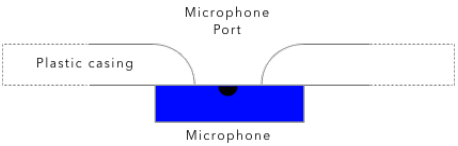

Figure 4.4 Microphone mounted in plastic casing.

Figure 4.5 Setup for industrial environment evaluation. Transmitter position marked with a black arrow.

with dimensions $4 \times 4 \times 2$ m^3. The transmitter was mounted on the end effector of a robot arm that could be moved within the volume, shown in Figure 4.5. For the first series the transmitter was moved to 12 different positions where distance measurements to all microphones were performed. The configuration of the microphone positions was changed to fit in a volume with dimensions $6 \times 4 \times 2$ m^3 and a second series of measurements for four additional transmitter positions were performed. The setup for the two series are shown in Figures 4.6 and 4.7. The true positions of the microphones and transmitter were determined with a Leica laser system [*Leica Viva TS16 - World's First Self-Learning Total Station*]. The transmitter sent a pseudo-

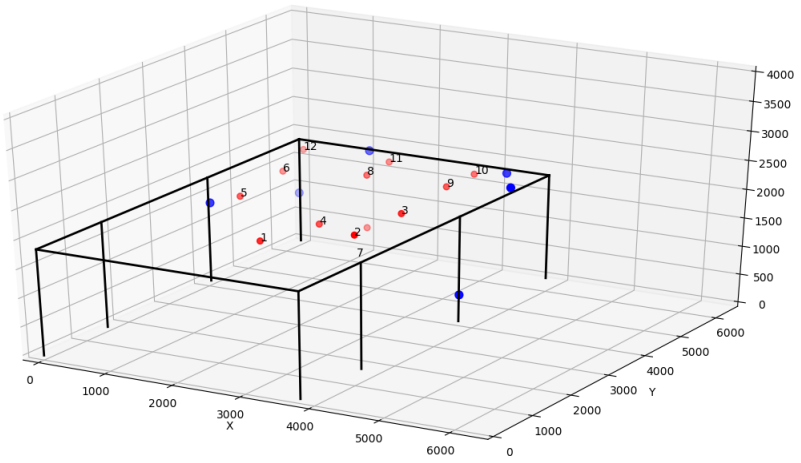

Figure 4.6 Microphone (blue) and transmitter (red) positions for series 1 [mm].

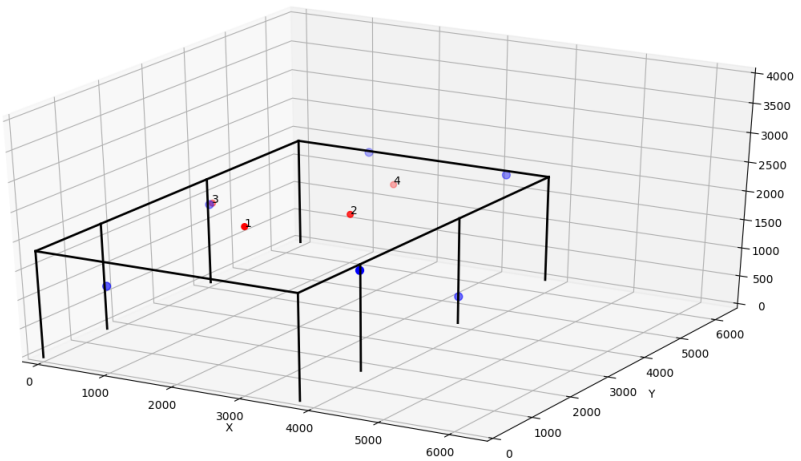

Figure 4.7 Microphone (blue) and transmitter (red) positions for series 2 [mm].

random noise signal of which the microphones recorded 20 ms 1-bit samples at 4M samples per second. The signal was converted to PCM and down-sampled to 100k samples per second. Fifty distance measurements between transmitter and each of the six microphones were performed at all transmitter positions. The distances were calculated with the recorded signal and the electrical signal sent to the transmitter as reference signal in the same manner as for the transmitter comparison process with two additions. The signal was filtered with a 16th-order Butterworth high-pass filter removing frequencies under 19 kHz. A Hilbert transform was applied to the cross-correlation signal before earliest peak search was performed. Values differing more than 4 mm from the most common value were considered outliers and were removed.
The distances were used in a numerical multilateration positioning algorithm together with the positions of the microphones and the position of the transmitter was calculated. The calculated distances and positions were compared to the true distances and true positions measured with the Leica system.

5

Results

5.1 Transmitter comparison

The results for the transmitter comparison using the electrical signal and the acoustic signal recorded with the microphone mounted at the robot as reference signal are presented below. The results are for the environment described in Section 4.1. The results and discussion for the corona discharge are presented in Appendix A as the evaluation process had to be modified and the results are not directly comparable.

Electrical reference signal

The results using the electrical signal as reference signal with the recorded signal are shown in Table 5.1. This is the combined absolute error for all positions in the evaluation process. The error and standard deviation for each position was divided with the true distance to that position to depict how the error varies by distance, seen as Mean/td and Std/td.

Emitter	Mean [mm]	Std [mm]	Mean/td [mm/mm]	Std/td [mm/mm]	Outliers removed
Piezo 1	34.61	6.49	0.11	0.05	264 (7.5%)
Piezo 2	11.04	1.92	0.04	0.01	199 (5.7%)
Piezo 3	11.56	3.08	0.04	0.02	195 (5.6%)
Piezo 4	26.59	44.35	0.06	0.02	236 (6.7%)
Piezo sphere	10.44	3.22	0.04	0.02	216 (6.2%)
Speaker 1	8.34	4.86	0.03	0.02	330 (9.4%)
Speaker 2	7.79	3.93	0.02	0.01	347 (9.9%)
Speaker 3	6.14	3.94	0.02	0.01	259 (7.4%)

Table 5.1 Mean and standard deviation for the combined error for the emitters, mean and standard deviation for the combined error divided by the true distance td and number of removed outliers when using electric reference signal.

Acoustic reference signal

The results using the signal recorded with the microphone mounted at the robot as reference signal are shown in Table 5.2. The introduced propagation delay from the transmitter to the reference microphone was corrected for.

Emitter	Mean [mm]	Std [mm]	Mean/td [mm/mm]	Std/td [mm/mm]	Outliers removed
Piezo 1	44.14	7.20	0.14	0.06	176 (5.0%)
Piezo 2	47.60	123.33	0.06	0.04	124 (3.5%)
Piezo 3	18.62	37.87	0.04	0.01	141 (4.0%)
Piezo 4	32.50	49.64	0.07	0.02	147 (4.2%)
Piezo sphere	38.34	36.96	0.12	0.11	294 (8.4%)
Speaker 1	10.61	3.89	0.03	0.02	307 (8.9%)
Speaker 2	14.58	4.92	0.05	0.02	727 (7.8%)
Speaker 3	12.07	3.45	0.04	0.02	216 (6.2%)

Table 5.2 Mean and standard deviation for the combined error for the emitters, mean and standard deviation for the combined error divided by the true distance td and number of removed outliers when using recorded reference signal.

The transmitter comparison process revealed Piezo 2 with electrical reference signal to have lowest standard deviation. Hence it was chosen for the industrial environment evaluation.

5.2 Industrial environment evaluation

Position	Mean absolute error [mm]	Error std [mm]	Outliers removed
1	1.1	1.5	7 (2.7%)
2	1.2	2.5	9 (3.6%)
3	1.7	2.2	5 (2.3%)
4	2.4	1.5	8 (2.4%)
5	3.3	1.2	9 (2.9%)
6	3.3	2.5	3 (0.9%)
7	124.1	169.4	11 (3.8%)
8	3.0	2.5	12 (3.8%)
9	2.9	2.3	7 (2.4%)
10	3.6	1.8	3 (1.2%)
11	3.3	2.3	17 (6.0%)
12	2.1	1.9	8 (2.7%)

Table 5.3 Distance measurement error, standard deviation and number of outliers removed for Series 1.

Series 1

The results from the distance measurements performed with Piezo 2 are shown in Table 5.3. The results from the positioning are shown in Table 5.4 and plotted in Figure 5.1.

Position	x	y	z
1	0.8	1.7	5.4
2	2.5	2.4	7.7
3	4.5	0.5	0.3
4	1.8	3.0	1.2
5	2.0	4.3	0.12
6	4.3	2.5	5.5
7	118.3	41.8	553.4
8	0.4	0.5	6.9
9	3.7	1.1	3.9
10	2.0	1.3	5.5
11	0.2	0.3	5.7
12	3.0	3.1	1.7

Table 5.4 Absolute error for each position in Series 1 [mm].

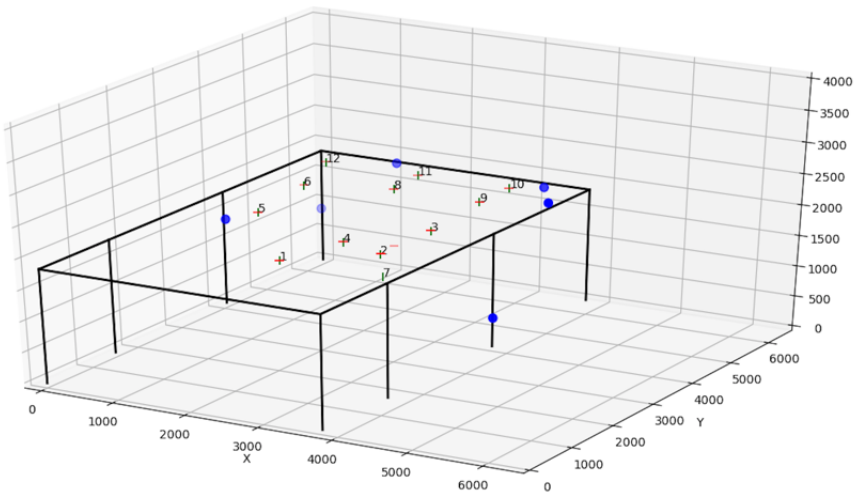

Figure 5.1 Microphone positions marked with blue dots. True transmitter positions marked with red bars. Calculated transmitter positions marked with green bars [mm].

Series 2

The results from the distance measurements performed with Piezo 2 are shown in Table 5.5. The results from the positioning are shown in Table 5.6 and plotted in Figure 5.2.

Position	Mean absolute error [mm]	Error std [mm]	Outliers removed
1	6.3	3.1	3 (0.9%)
2	5.4	2.6	3 (1.0%)
3	4.9	2.6	7 (3.9%)
4	4	1.5	20 (6.0%)

Table 5.5 Distance measurement error, standard deviation and number of outliers removed for Series 2.

Position	x	y	z
1	2.2	6.9	5.9
2	3.4	1.0	5.5
3	6.3	2.3	6.7
4	1.9	1.4	8.4

Table 5.6 Absolute error for each position in Series 2 [mm].

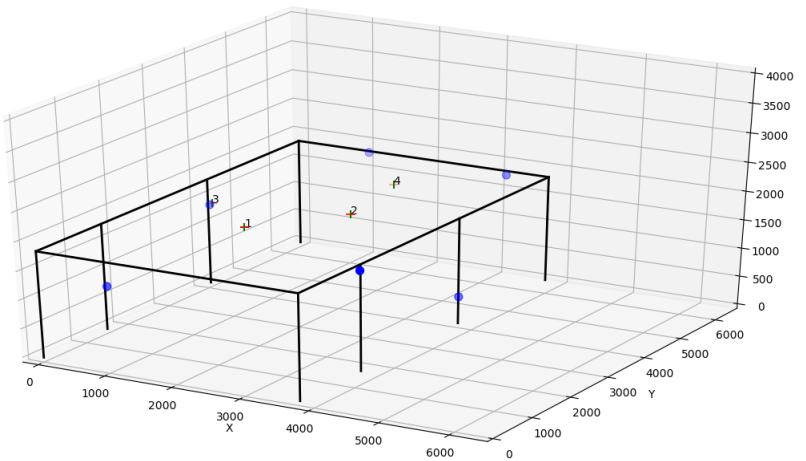

Figure 5.2 Microphone positions marked with blue dots. True transmitter positions marked with red bars. Calculated transmitter positions marked with green bars [mm].

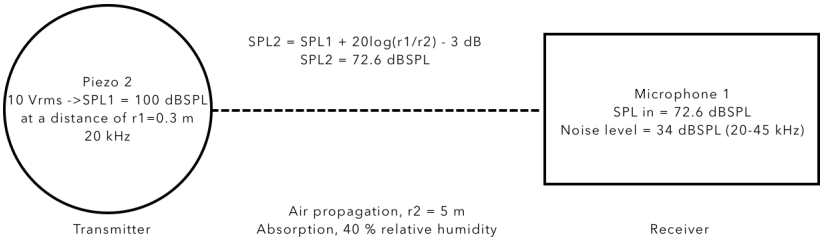

Figure 5.3 Link budget for a system using Piezo 2 and Microphone 1 separated with a distance of 5 m.

5.3 Discussion

Electric and acoustic reference signal

Using the electric signal as reference signal is the least complex solution. The setup with acoustic signal as reference signal was tested to see if the results could be improved. Using the acoustic signal as reference could for example mitigate the negative effects that can be introduced by distortions caused by the transmitter. The added complexity of the setup does however seem to cancel any such improvements.

Mean error difference

The mean error for Piezo 2 in the transmitter comparison process and the industrial environment evaluation differs. This is likely due to the difference in the hardware setup causing different delays introduced by the amplifier, transmitter group delay and ADC/DAC as well as different physical dimensions of transmitter and microphone mountings.

Series 1, position 7

After examining the evaluation setup it emerged that several receivers were not in line-of-sight from the transmitter. This was caused by the robot obstructing the direct path. As a consequence the direct wave was attenuated and had to travel the longer way around the object leading to incorrect distances being calculated. It is also possible reflected waves were first to reach the receiver and the distances calculated became longer than the true direct path distance.

SNR

Figure 5.3 shows a link budget, i.e. how the SNR changes through the system, for a system using Piezo 2 and Microphone 1 separated with a distance of 5 m. At this distance the budget shows that the resulting SNR at the receiver should be high enough for the signal to be interpreted both at 0 degrees and at an 125 ($\pm$62.5) degree angle (-6 dB).

Measurement angle

Successful distance measurements were performed at angles up to ± 98 degrees. Measurements with wider angles were not possible due to the direct path being obstructed by the robot actuator.

Outliers

Examination of the outliers from the transmitter evaluation processes points to interference from reflected waves leading to false max correlation peaks and/or wrong peak being chosen by the early peak search algorithm as main causes.

The majority of the outliers from the industrial environment evaluation were caused by an issue with the time synchronization. Examination points to 8 (0.2%) of the outliers in Series 1 and 15 (1.3%) of the outliers in Series 2 being caused by low SNR leading to either the wrong peak being chosen by the early peak search algorithm or reflecting waves interfering causing false max peaks.
Due to radio issues some of the distance measurement data was corrupted when transfered between receiver and transmitter. These measurements are not included and hence the actual number of distance measurements per position varied between 179 and 300 which can be seen from the percentage values in Table 5.3 and Table 5.5.

Accuracy

By varying the temperature it can be seen that the worst case of 0.5 degree temperature difference can generate up to 0.2 m/s speed difference when using Equation 2.2. For distance measurements between 2 and 5 meters this leads to a variable error up to 1.8 mm. The method for how to calculate the speed of sound in air is under debate which can add to the error [Cramer, 1993] [Wong, 1995]. The acoustic center for the transmitter and receivers used should be measured to ensure correct measurement reference points.

6

Conclusion and future work

Distance measuring system

A distance measurement system using a ultrasound transmitter and MEMS microphones was developed. Evaluation shows sub-centimeter accuracy for line-of-sight wide-angle measurements in an industrial environment over a wide range of directions.

Future work

If the speed of sound is calculated from environmental properties additional and more accurate temperature sensors should be used. A method for determining the speed of sound in a more direct way, as described in Section 2.1, could be used.

Porting variations for the transmitters and microphones should be explored to increase efficiency and transmission/reception angle.

The piezo sphere offers exiting possibilities due to its resemblance to the ideal source, a pulsating sphere, and should be further explored for omni-directional purposes with need for a well defined acoustic center.

A

Corona discharge transmitter

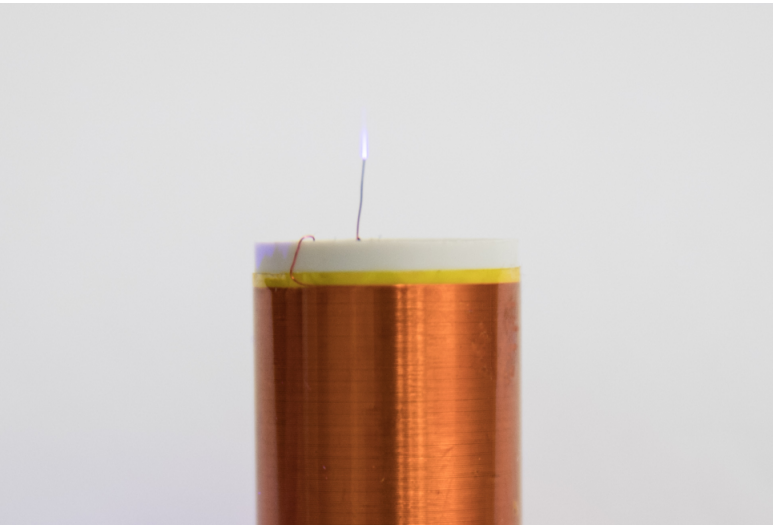

Figure A.1 Corona discharge.

A corona discharge was created around the tip of a 0.13 mm thick copper wire and modulated to produce sound, shown in Figure A.1. The small size of the corona makes the transmitter very interesting as it is essentially a point source. The size is in the range of what could be considered a simple source for ultrasound frequencies and should be omni-directional.
There were issues capturing data for some of the positions during the transmitter comparison process. For the positions depicted in Figure 4.2-1 at heights 100 and 150 mm, no data could be captured. This was likely due to the microphone being

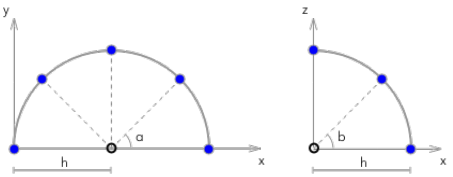

Figure A.2 Evaluation positions. Transmitter position depicted as a black hollow dot and microphone position for each measurement depicted as a blue dot.

affected by the electric and magnetic fields caused by the corona discharge transmitter. For the positions depicted in Figure 4.2-3 at the angle α equal to 50 degrees and the positions depicted in Figure 4.2-6 the cause for no data being accurately captured was most likely due to the low output of the transmitter resulting in too low SNR. The results, with the positions causing errors redacted, are presented in Table A.1.

The corona discharge transmitter was additionally evaluated in an anechoic chamber for the positions shown in Figure A.2. The angle a was varied between 0 and 180 degrees at 45 degree steps. At a equal to 0, the angle b was varied between 0 an 90 degrees at 45 degree steps. The distance h was 500 mm for all measurements. 100 measurements were performed at each position and the distance was calculated as described in Section 4.1 with the electrical signal as reference. The mean error and standard deviation for each position are shown in Table A.2.

Results

Reference signal	Mean [mm]	Std [mm]	Mean/td [mm/mm]	Std/td [mm/mm]	Outliers removed
Electric	7.37	1.26	0.02	0.00	50 (1.7%)
Acoustic	70.53	2.61	0.23	0.04	53 (1.8%)

Table A.1 Results for the transmitter comparison using the corona discharge as transmitter. Mean absolute error, error standard deviation, mean error and error standard deviation divided by the true distance td and outliers removed.

Using a corona discharge as transmitter is viable, in particular if the output is increased. Care must be taken as it requires high voltages and a small amount of ozone usually is a by product of operation. Higher accuracy could be achieved by modifying the point around which the corona forms. This could result in a transmitter with a very well defined acoustic center.

a	b	Mean absolute error [mm]	Error std [mm]	Outliers removed
0	0	7.2	0.09	0
45	0	6.1	0.09	0
90	0	4.3	0.14	0
135	0	8.0	0.06	0
180	0	6.5	0.07	0
0	45	9.3	0.08	2 (2%)
0	90	8.2	0.09	0

Table A.2 Mean absolute error, standard deviation and outliers removed for each position shown in Figure A.2.

Bibliography

A. Olshausen, B. (2000). *Aliasing*. URL: http://redwood.berkeley.edu/bruno/npb261/aliasing.pdf (visited on 2017-08-23).

Ali-Löytty, S., J. Collin, and N. Sirola (2010). *MAT-45806 Mathematics for positioning & MAT-45807 Mathematics for positioning*. Tampere University of Technology, Department of Mathematics. Tampere, Finland.

Beranek, L. L. (1986). *Acoustics*. Published by the American Institute of Physics for the Acoustical Society of America, New York, N.Y. ISBN: 978-0-88318-494-3.

BME280. URL: https://www.bosch-sensortec.com/bst/products/all_products/bme280 (visited on 2017-07-13).

Chizhov, M., M. Eingorn, and V. Kulinskii (2013). "Stable sound wave generation in weakly ionized air medium". *arXiv preprint arXiv:1304.7792*. URL: https://arxiv.org/abs/1304.7792 (visited on 2017-03-12).

Cramer, O. (1993). "The variation of the specific heat ratio and the speed of sound in air with temperature, pressure, humidity, and CO_2 concentration". *The Journal of the Acoustical Society of America* **93**:5, pp. 2510–2516. ISSN: 0001-4966. DOI: 10.1121/1.405827. URL: http://asa.scitation.org/doi/10.1121/1.405827 (visited on 2017-03-01).

Engineering Acoustics/Outdoor Sound Propagation - Wikibooks, open books for an open world. URL: https://en.wikibooks.org/wiki/Engineering_Acoustics/Outdoor_Sound_Propagation (visited on 2017-09-06).

Hexagon, G. *Leica Viva TS16 - World's First Self-Learning Total Station*. URL: http://leica-geosystems.com/en-us/products/total-stations/robotic-total-stations/leica-viva-ts16 (visited on 2017-07-05).

Kester, W. (2004). *Analog-digital conversion*. English. OCLC: 69252274. Analog Devices. ISBN: 978-0-916550-27-1.

Kleiner, M. (2013). *Electroacoustics*. Taylor & Francis, Boca Raton, FL. ISBN: 978-1-4398-3618-7.

MATLAB R2016b. Natick, Massachusetts, United States. URL: https://se.mathworks.com/products/new_products/release2016b.html (visited on 2017-06-12).

Medina, C., J. Segura, and A. De la Torre (2013). "Ultrasound Indoor Positioning System Based on a Low-Power Wireless Sensor Network Providing Sub-Centimeter Accuracy". en. *Sensors* **13**:3, pp. 3501–3526. ISSN: 1424-8220. DOI: 10.3390/s130303501. URL: http://www.mdpi.com/1424-8220/13/3/3501/ (visited on 2017-08-17).

open_abb (2017). *Open_abb: Control ABB robots remotely*. original-date: 2012-05-21T18:44:15Z. URL: https://github.com/robotics/open_abb.

Oppenheim, A. V., R. W. Schafer, and J. R. Buck (1999). *Discrete-time signal processing*. 2nd ed. Prentice Hall, Upper Saddle River, N.J. ISBN: 978-0-13-754920-7.

RME: Fireface UFX. URL: http://www.rme-audio.de/en/products/fireface_ufx.php (visited on 2017-07-12).

Robotdalen. URL: http://www.robotdalen.se/en (visited on 2017-09-13).

Saad, M. M., C. J. Bleakley, and S. Dobson (2011). "Robust High-Accuracy Ultrasonic Range Measurement System". *IEEE Transactions on Instrumentation and Measurement* **60**:10, pp. 3334–3341. ISSN: 0018-9456, 1557-9662. DOI: 10.1109/TIM.2011.2128950. URL: http://ieeexplore.ieee.org/document/5749694/ (visited on 2017-01-24).

Thrane, N. "Technical Review To Advance Techniques in Acoustical, Electrical and Mechanical Measurement - The Hilbert Transform". URL: https://bksv.com/media/doc/bv0015.pdf (visited on 2017-09-08).

Thrane, N., J. Wismer, H. Konstantin-Hansen, and S. Gade. "Practical use of the "Hilbert transform"". URL: https://www.bksv.com/media/doc/bo0437.pdf (visited on 2017-07-18).

Thrun, S., W. Burgard, and D. Fox (2005). *Probabilistic robotics*. Intelligent robotics and autonomous agents. OCLC: ocm58451645. MIT Press, Cambridge, Mass. ISBN: 978-0-262-20162-9.

Wong, G. S. K. (1995). "Comments on "The variation of the specific heat ratio and the speed of sound in air with temperature, pressure, humidity, and CO_2 concentration" [J. Acoust. Soc. Am. 93, 2510–2516 (1993)]". en. *The Journal of the Acoustical Society of America* **97**:5, pp. 3177–3179. ISSN: 0001-4966. DOI: 10.1121/1.411818. URL: http://asa.scitation.org/doi/10.1121/1.411818 (visited on 2017-03-01).

Lund University
Department of Automatic Control
Box 118
SE-221 00 Lund Sweden

Document name
MASTER'S THESIS

Date of issue
September 2017

Document Number
TFRT-6040

Author(s)
Ivar Bergkvist

Supervisor
Peter Isberg, Sony Mobile
Anders Robertsson, Dept. of Automatic Control, Lund University, Sweden
Rolf Johansson, Dept. of Automatic Control, Lund University, Sweden (examiner)

Title and subtitle

A high-accuracy wide-angle acoustic system for distance measurements and robot positioning

Abstract

Wide-angle distance measurements are needed for positioning with multilateration when there is no information about in which direction objects of interest are located. Several transmitters of varying kinds were evaluated in a data-driven way using a 6 DOF robot actuator. A wide-angle (±98 degrees) distance measurement system using ultrasound was developed. The resulting solution was integrated in a positioning system showing sub-centimeter accuracy in an industrial environment.

Keywords

Classification system and/or index terms (if any)

Supplementary bibliographical information

ISSN and key title
0280-5316

ISBN

Language
English

Number of pages
1-48

Security classification